

Article

Influence of Tempering Temperature and Time on Microstructure and Mechanical Properties of Additively Manufactured H13 Tool Steel

Kichang Bae ¹, Hyoung-Seok Moon ², Yongho Park ³, Ilguk Jo ^{4,*} and Junghoon Lee ^{1,*}¹ Department of Metallurgical Engineering, Pukyong National University, Busan 48513, Republic of Korea² Advanced Energy Materials and Components R&D Group, Korea Institute of Industrial Technology, Busan 46938, Republic of Korea³ Department of Materials Science and Engineering, Pusan National University, Busan 46241, Republic of Korea⁴ Department of Advanced Materials Engineering, Dong-Eui University, Busan 47340, Republic of Korea* Correspondence: ijo@deu.ac.kr (I.J.); jlee1@pknu.ac.kr (J.L.)

Abstract: Among various processes for manufacturing complex-shaped metal parts, additive manufacturing is highlighted as a process capable of reducing the wastage of materials without requiring a post-process, such as machining and finishing. In particular, it is a suitable new manufacturing technology for producing AISI H13 tool steel for hot-worked molds with complex cooling channels. In this study, we manufactured AISI H13 tool steel using the laser power bed fusion (LPBF) process and investigated the effects of tempering temperature and holding time on its microstructure and mechanical properties. The mechanical properties of the sub-grain cell microstructure of the AISI H13 tool steel manufactured using the LPBF process were superior to that of the H13 tool steel manufactured using the conventional method. These sub-grain cells decomposed and disappeared during the austenitizing process; however, the mechanical properties could be restored at a tempering temperature of 500 °C or higher owing to the secondary hardening and distribution of carbides. Furthermore, the mechanical properties deteriorated because of the decomposition of the martensite phase and the accumulation and coarsening of carbides when over-tempering occurred at 500 °C for 5 h and 550 °C for 3 h.

Keywords: additive manufacturing; laser powder bed fusion; AISI H13 tool steel; post-heat treatment; tempering



Citation: Bae, K.; Moon, H.-S.; Park, Y.; Jo, I.; Lee, J. Influence of Tempering Temperature and Time on Microstructure and Mechanical Properties of Additively Manufactured H13 Tool Steel. *Materials* **2022**, *15*, 8329. <https://doi.org/10.3390/ma15238329>

Academic Editor: Adam Grajcar

Received: 23 October 2022

Accepted: 20 November 2022

Published: 23 November 2022

Publisher's Note: MDPI stays neutral with regard to jurisdictional claims in published maps and institutional affiliations.



Copyright: © 2022 by the authors. Licensee MDPI, Basel, Switzerland. This article is an open access article distributed under the terms and conditions of the Creative Commons Attribution (CC BY) license (<https://creativecommons.org/licenses/by/4.0/>).

1. Introduction

Additive manufacturing (AM) is a process of directly fabricating a final product by stacking objects in a layer-by-layer manner using a computer-aided three-dimensional design [1–4]. With the advent of the fourth industrial revolution, the process is gaining attention as an innovative technology that can change the manufacturing industry because of the easy manufacturing of complex-shaped products that are difficult to manufacture using conventional processes. Metal AM is a process of printing products using metal powder or metal wire. The metal parts produced by AM can be used in various industries, such as the automobile, structural material, aerospace, medical, and remanufacturing fields [5–8]. Directed energy deposition (DED) and powder bed fusion (PBF) are the commonly used metal AM processes. In particular, the PBF process is primarily used to manufacture multiple small and complex products simultaneously. Among the various energy sources, the laser powder bed fusion (LPBF) process uses a laser beam as a heat source for melting metal powder and demonstrates excellent shape accuracy. Several studies have been conducted on the LPBF process to manufacture excellent final products by combining various process parameters such as laser power, laser scanning speed, and type of metal powder [9–11].

AISI H13 tool steel (H13), known as hot-worked mold steel, is widely used in molds with cooling channels, such as die casting, plastic injection molds, forging, and extrusion because of its high-temperature strength, ductility, excellent tempering resistance, and wear resistance [12–14]. The H13 mold is conventionally manufactured by the subtractive processing of large H13 blocks. However, due to the high hardness of the H13, it is difficult to create complex shapes and cooling channels by cutting and machining with tools [15,16]. Moreover, the subtractive process incurs a significant cost, time, and wastage of material. In contrast, the LPBF process can overcome these limitations. Complex-shaped molds and cooling channels in molds, which improve the quality of the product and the lifetime of the mold, can be created using the LPBF process of mold metals. These advantages of the LPBF process for applications to metal mold fabrication have triggered extensive studies on the optimization of LPBF of mold metals.

Problems such as porosity, cracking, and high residual stresses can occur due to rapid cooling (approximately 10^{6-7} K/s) during the manufacturing of H13 using the AM process [17–19]. To solve these problems, various post-treatment processes using hot isostatic pressing (HIP) and heat treatment (HT) have been developed. HT, especially, can efficiently resolve these problems via microstructure changes. Therefore, the effects of the process parameters of AM and post-HT on the microstructure and mechanical properties of H13 manufactured using the AM process need to be understood. Several studies have been conducted to analyze the microstructure and mechanical properties of H13 manufactured using AM and the effects of post-HT. Åsberg et al. [20] studied the effect of post-treatment on the microstructure, pores, and mechanical properties of H13 manufactured using the LPBF process. They suggested that post-treatment using HIP could reduce pores and fusion defects, thereby improving the mechanical properties. Yuan et al. [21] reported the effect of the post-treatment on the tensile and impact toughness properties of H13 manufactured using the LPBF process. They revealed that the direct tempering of H13, showing more dispersal of carbide, resulted in a lower thermal softening than conventional post-HT of H13, which includes a solution treatment before the tempering. Wang et al. [22] investigated the effect of a double-tempering HT on the thermal fatigue properties of H13 manufactured using a selective laser melting (SLM) process, which fully melts the metal powder. The H13 manufactured using the SLM showed a superior thermal fatigue resistance compared to the forged H13 due to its fine microstructure and higher amount of retained austenite. The relationship between the microstructure changes by post-HT and the mechanical properties of the H13 manufactured using the AM process has been extensively explored. Evaluation of various post-HT processes is crucial in the practical applications of the H13 manufactured by the AM process.

In this study, we applied various tempering temperatures and times to H13 steel manufactured using SLM, which is one of the LPBF processes, then the effects of tempering temperature and time on microstructure and mechanical properties were investigated by comparing as-built. Tempering temperature and time were used as variables after the solution treated H13.

2. Materials and Methods

Based on the PBF process, specimens were printed using the LPBF process using Mlab Cushing R (Concept Laser, GE, Boston, MA, USA) with Nd:YAG fiber laser (wavelength: 1064 nm) as a heat source. Spherical gas-atomized H13 steel powder (Sandvik Osprey Ltd., Sandviken, Sweden) with an average particle diameter of $-47\ \mu\text{m}$ was used to fabricate the specimens used in this study. The chemical compositions of H13 steel powder are listed in Table 1.

Table 1. Chemical compositions of H13 tool steel.

Elements	Fe	Cr	Mo	Mn	Si	V	C
wt.%	Bal.	5.13	1.60	0.47	1.08	1.15	0.41

The morphology of the H13 powder (see Figure 1a) was observed using field-emission scanning electron microscopy (FE-SEM, MIRA 3, Tescan, Brno, Czech Republic), a particle size analyzer (PSA, LS 320, BouLA, BoulAcer) was used to measure the average particle diameter of H13 powder (Figure 1b). An LPBF process was performed in an N₂ (g) atmosphere with an oxygen concentration of less than 1% to prevent oxidation of the specimen. A 90° rotate scanning strategy was used between each layer (see Figure 1c). The detailed parameters of LPBF used in this study are listed in Table 2.

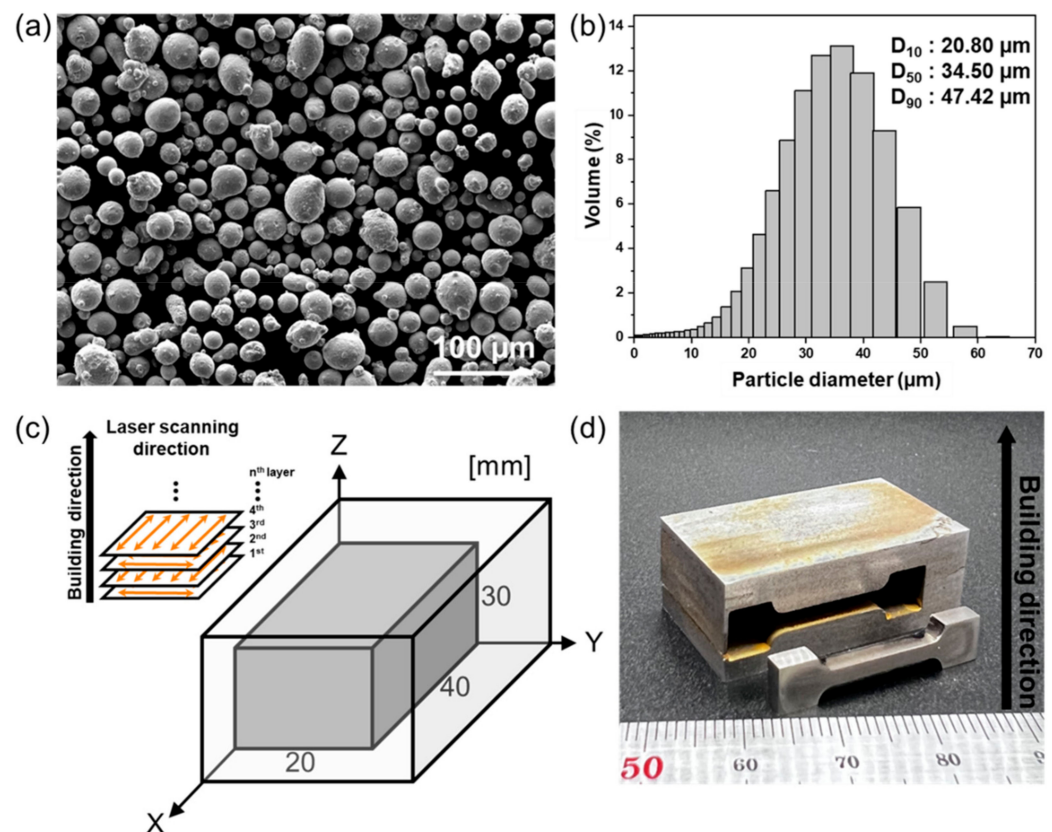


Figure 1. (a) Morphology and (b) particle size analysis of AISI H13 powder steel. (c) Schematic illustrations of the LPBF process and (d) printed sample and tensile specimen images.

Table 2. Parameters used for the LPBF process of H13 tool steel.

Parameters	Values
Laser power (W)	90
Scanning speed (mm/s)	800
Lamination thickness (mm)	0.025
Overlap (%)	30

Specimens were built in a rectangular shape of 20 × 40 × 30 mm³ to evaluate the microstructure and mechanical properties of the post-heat treatment process of the H13 tool steel manufactured using the LPBF. Heat treatment was performed in an Ar (g) atmosphere using a horizontal tubular furnace to observe changes in the microstructure and mechanical properties of the post-heat treatment specimen. Solution treatment was performed at 1000 °C for 1 h, and tempering heat treatment was conducted at 200, 300, and 500 °C for 2, 3, and 5 h, respectively. H13 steel is known to cause secondary hardening around 500 °C. Therefore, 200 °C, which is a relatively lower temperature, and 500 °C and 550 °C, which are the temperatures at which secondary hardening occurs, were selected. After solution treatment, the specimen was oil quenched (O.Q.), and the tempering heat-treated specimen

was cooled by air cooling (A.C.). Specimen notations according to each heat treatment condition are shown in Table 3.

Table 3. Various post-heat treatment conditions of the H13 manufactured by the LPBF process.

Sample Name	Solution Treatment Temperature (°C)	Time (h)	Cooling	Tempering Temperature (°C)	Time (h)	Cooling
as-built	-	-	-	-	-	-
S1000	1000	1	O.Q.	-	-	-
T2002	1000	1	O.Q.	200	2	A.C.
T2003	1000	1	O.Q.	200	3	A.C.
T2005	1000	1	O.Q.	200	5	A.C.
T5002	1000	1	O.Q.	500	2	A.C.
T5003	1000	1	O.Q.	500	3	A.C.
T5005	1000	1	O.Q.	500	5	A.C.
T5502	1000	1	O.Q.	550	2	A.C.
T5503	1000	1	O.Q.	550	3	A.C.

Phase analysis was analyzed using X-ray diffraction (XRD, Ultima IV, Rigaku, Tokyo, Japan) in the range of 2θ between 10° and 90° using the Mo target ($K\alpha = 0.7093 \text{ \AA}$) under the condition of an acceleration voltage of 30 kV, current of 40 mA, and scanning speed of $1.2^\circ/\text{min}$. For microstructure observation, micro-polishing was performed down to $1 \mu\text{m}$ in each specimen, and etching was conducted using Viella's agent (1 g picric acid, 5 mL HCl, and 95 mL ethanol). The microstructure of each specimen was observed using FE-SEM.

Hardness and tensile tests were performed to study the mechanical properties of the H13 manufactured using the LPBF process. For the hardness test, a Digital Rockwell hardness tester (MV-1, MATSUZAWA, Akita, Japan) was used, 10 hardness measurements were carried out for each specimen, and an average value was used. A universal testing machine (RB301, UNITECH-T, R&B Inc., Daejeon, Republic of Korea) was used to evaluate tensile properties. Tensile specimens were machined in a direction perpendicular to the built direction from specimens prepared using the H13 manufactured by the LPBF process (Figure 1d) with ASTM E8 standard for plate-type sub-sized specimens (gauge length = 13.2 mm, thickness = 2 mm). Micro-polishing of the tensile specimen was performed down to $1 \mu\text{m}$. A tensile test was conducted at a strain rate of $1.0 \times 10^{-3} \text{ s}^{-1}$, and strain gauges were attached to the specimens for elongation measurements. A tensile test was conducted in the atmospheric atmosphere at room temperature, and FE-SEM was used for fracture surface observation after the tensile test.

To minimize the experimental error in hardness, elongation, and tensile strength, we used seven samples fabricated by each condition. Excluding maximum and minimum values, five results were averaged. Then, stress–strain curves, which have the most similar values (i.e., ultimate tensile strength and elongation) to average, were shown as representative results.

3. Results and Discussion

XRD analysis was performed to examine the phase changes according to the HT conditions, and the results are shown in Figure 2. The peaks of the α' -martensite and $(\text{Cr,Fe})_7\text{C}_3$ carbide (M_7C_3) are observed in all specimens. The M_7C_3 is speculated to form in the H13 matrix because of the rapid solidification during the LPBF process. M_7C_3 has a hexagonal close-packed structure. These carbides are thermally unstable at high temperatures and easily precipitate, decompose, and grow [23]. Conversely, the γ -austenite phase is observed only in the as-built specimen, which corresponds to the retained austenite in the matrix due to the rapid cooling during the LPBF process. These retained austenite indicate the incomplete transformation from austenite to martensite during the cooling of as-built H13 [24,25]. This peak related to the γ -austenite phase is not observed in the post-HT samples, indicating that the γ -austenite phase disappears due to the solution treatment.

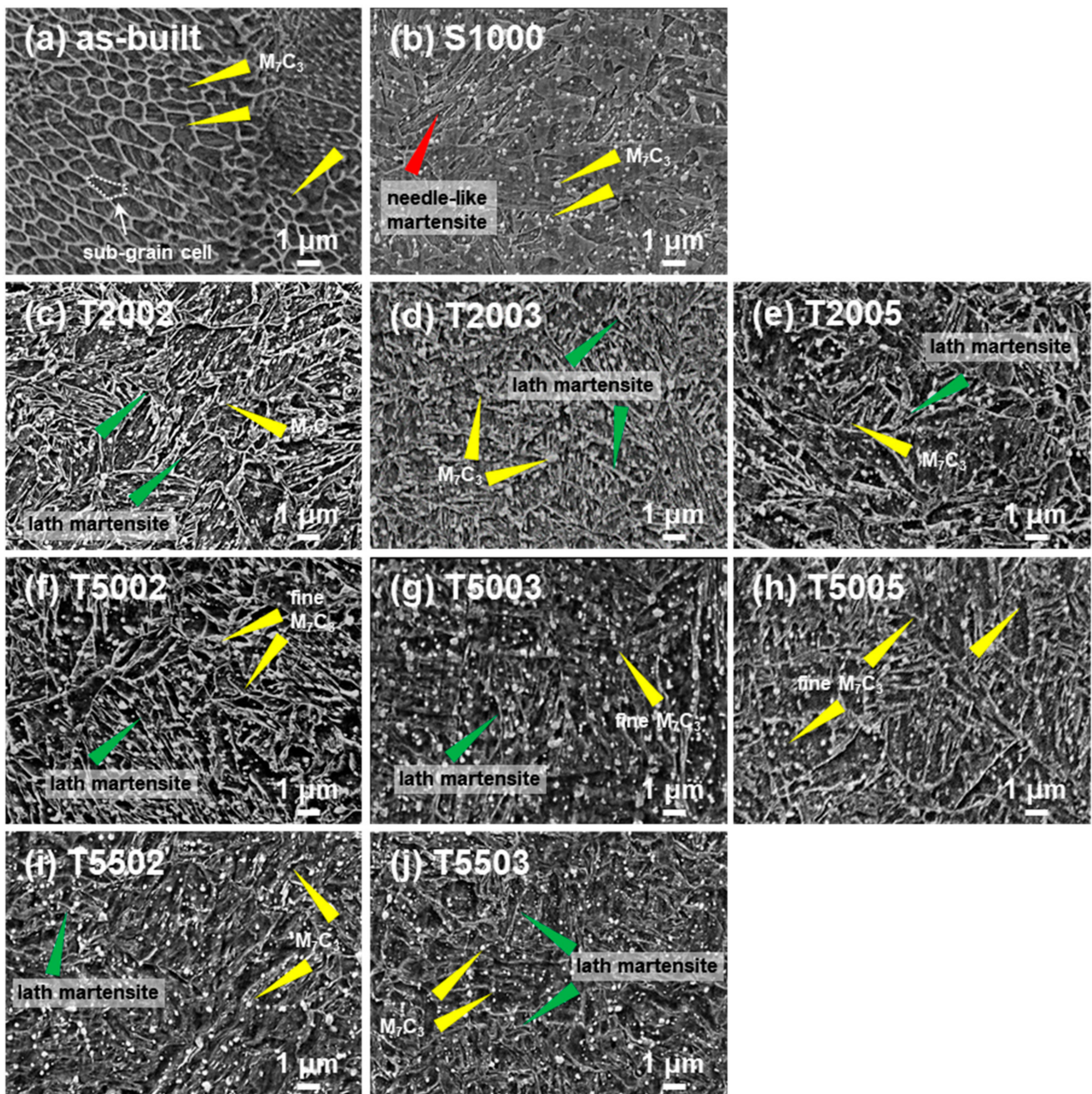


Figure 3. FE-SEM images of the microstructure of each specimen according to the heat treatment conditions.

The hardness and tensile tests were conducted to investigate the effects of these microstructure changes on the mechanical properties of H13 manufactured using the LPBF process. Figure 4 shows the hardness test results of the H13 manufactured using the LPBF process at different tempering temperatures and times. Among the H13 manufactured using the LPBF process, the as-built specimen shows the highest hardness of 47.5 HRC. The high hardness is attributed to the sub-grain cells and the M_7C_3 formed during the AM process [29]. The hardness of S1000 decreases to 43.2 HRC due to the decomposition and disappearance of the sub-grain cells during the austenitizing HT. The specimens T2002, T2003, and T2005, tempered at a low temperature of 200 °C, show a reduction in hardness, suggesting that secondary hardening does not occur at low temperature. A slight increase in the hardness is observed with the increasing holding time at the tempering

temperature of 200 °C. The hardness of T5002, T5003, T5005, T5502, and T5503 specimens, where secondary hardening occurs, are observed to be different at different tempering treatment times. The T5002, T5003, and T5502 specimens recover their hardness to 46, 46.4, and 47 HRC, respectively, which is similar to that of the as-built specimen because of the secondary hardening during the tempering process; however, the hardness of T5005 and T5503 decrease to 42.4 and 41.2 HRC, respectively. Therefore, the H13 manufactured using the LPBF process is considered over-tempered at tempering conditions of 500 °C for 5 h and 550 °C for 3 h. This is because of the gathering and coarsening of the finely dispersed M_7C_3 under these tempering HT conditions [30–32].

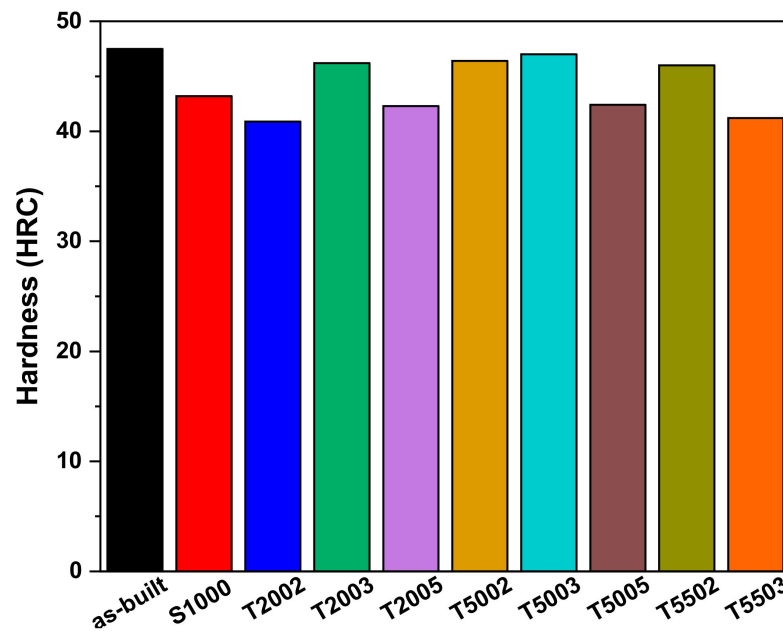


Figure 4. Average hardness of each specimen according to the heat treatment conditions.

Tensile tests of the T5003, T5502, and T5503 specimens, selected based on the hardness test results, were conducted, and results were compared with those of the as-built specimens. Figures 5 and 6 show the stress–strain curve and the fracture surface of the as-built, T5003, T5502, and T5503 specimens, respectively. Regardless of the post-HT, all tensile specimens undergo fractures before any plastic deformation occurs. The as-built specimen shows an ultimate tensile strength (UTS) of 1245 MPa and a strain of 9.49% (Figure 5a), thereby suggesting the best tensile properties. Only a cleavage fracture (yellow triangle in Figure 6a) is observed, indicating a typical brittle fracture [33,34]. The hardness of T5003 is similar to that of the as-built specimen; however, the UTS is 1126 MPa, which is 90% of that of the as-built specimen. Furthermore, fine dimples (green triangle in Figure 6b) are observed around the cleavage fracture in the fracture surface of the T5003 (Figure 6b) [35], which is different from that of the as-built specimen. These fine dimples are produced as fracture progress around the M_7C_3 . When tempering is performed at 500 °C, the secondary hardening does not sufficiently progress, thereby resulting in a fracture at a low UTS during the tensile test. Conversely, the UTS of the T5502 specimen, which has a similar hardness to the as-built specimen, is 1246 MPa; however, the strain decreases to 7.49%. In addition, the fracture surface of the T5502 is observed to primarily contain the cleavage fracture (Figure 6c), similar to the as-built specimen. However, a few fine dimple fractures are also observed, attributed to the improved UTS of the T5502 because of the sufficient secondary hardening during tempering treatment at 550 °C for 2 h. The strain of the T5503 specimen is 7.46%, similar to that of the T5502, whereas the UTS decreases to 1078 MPa. The fracture surface demonstrates a fractography similar to that of the T5003. The observations indicate the decomposition of the lath martensite and coarsening of the finely dispersed M_7C_3 during

the tempering at 550 °C for 3 h. The H13 manufactured using the LPBF process maintained the highest hardness and tensile strength, which are similar to those of the as-built specimen when post-HT condition of T5502.

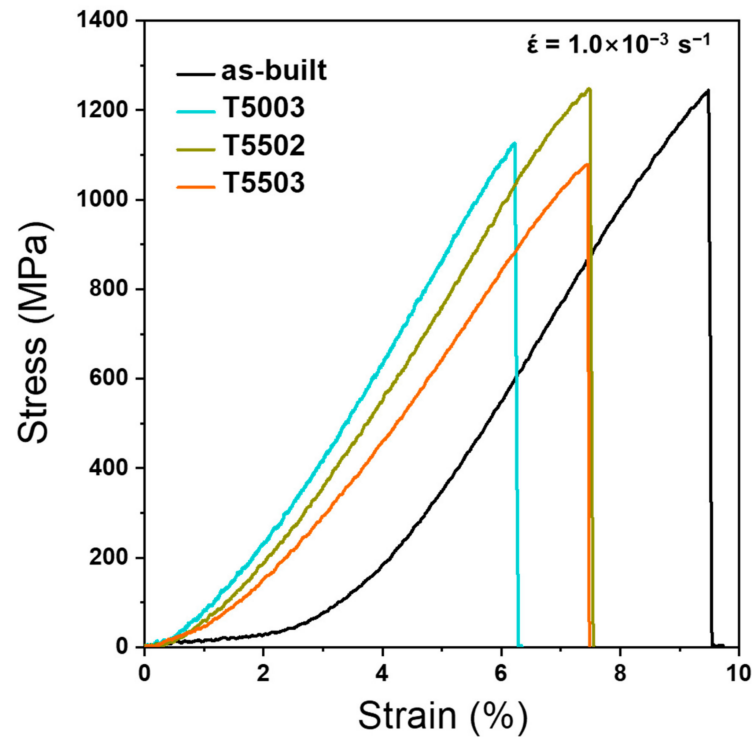


Figure 5. Tensile stress–strain curves of the as-built, T5003, T5502, and T5503 specimens.

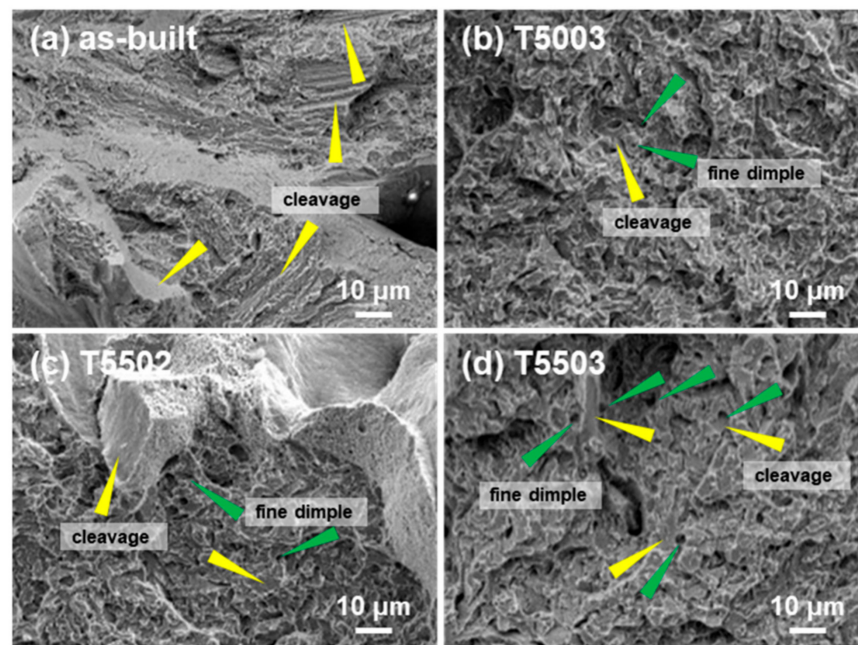


Figure 6. Fracture surface of (a) as-built, (b) T5003, (c) T5502, and (d) T5503 specimens.

Commercial forged H13 steels have been reported to have UTS of 1200–1590 MPa, elongation of 6–9%, and hardness of 46–50 HRC [22,36–38]. Regarding these mechanical properties of commercially forged H13, additively manufactured H13 using the LPBF process did not show significant differences in this study. Nevertheless, it should be

noted that the LPBF process has an advantage in complex shape fabrication with metals. Therefore, even though the LPBF process cannot significantly improve the mechanical properties of H13, understanding the effects of post-HT in microstructure and mechanical properties of additively manufactured H13 would be valuable in designing and producing metal molds with H13 using the LPBF process.

4. Conclusions

H13 manufactured using the LPBF process showed superior mechanical properties without post-HT due to the sub-grain cells. The sub-grain cell structure decomposed and disappeared during solution treatment. A significantly lower hardness was observed when the H13 was tempered at 200 °C than the as-built specimen, which can be attributed to the insufficient secondary hardening at low temperature. When tempering was performed at 500 °C and 550 °C, the hardness could be recovered, indicating that a sufficiently high temperature is required for secondary hardening. In addition, the M_7C_3 formed during the LPBF process was finely dispersed in the matrix at a tempering temperature of 500 °C or higher, thereby improving the mechanical properties of the H13. However, when tempering was performed at 500 °C for 5 h or at 550 °C for 3 h, the M_7C_3 gathered and coarsened, resulting in a deterioration of the mechanical properties. Therefore, when a post-HT process is designed to improve the mechanical properties of H13 manufactured using the LPBF process, the microstructure changes and secondary hardening by the M_7C_3 should be fully understood.

Author Contributions: Conceptualization, K.B., I.J. and J.L.; Funding acquisition, J.L.; Investigation, K.B., H.-S.M. and Y.P.; Writing—original draft preparation, K.B.; Writing—review and editing I.J. and J.L. All authors have read and agreed to the published version of the manuscript.

Funding: This work is supported by the Advanced Technology Center Development Program (Grant No. 20008753), funded by the Ministry of Trade, Industry, and Energy.

Conflicts of Interest: The authors declare no conflict of interest.

References

1. Milewski, J.O. *Additive Manufacturing of Metals*; Springer: Berlin/Heidelberg, Germany, 2017; Volume 258.
2. Yakout, M.; Elbestawi, M.A.; Veldhuis, S.C. A Review of Metal Additive Manufacturing Technologies. *Solid State Phenom.* **2018**, *278*, 1–14. [[CrossRef](#)]
3. Singh, S.; Ramakrishna, S.; Singh, R. Material issues in additive manufacturing: A review. *J. Manuf. Process.* **2017**, *25*, 185–200. [[CrossRef](#)]
4. Ngo, T.D.; Kashani, A.; Imbalzano, G.; Nguyen, K.T.Q.; Hui, D. Additive manufacturing (3D printing): A review of materials, methods, applications and challenges. *Compos. Part B Eng.* **2018**, *143*, 172–196. [[CrossRef](#)]
5. Srivastava, M.; Rathee, S.; Maheshwari, S.; Kundra, T. *Additive Manufacturing: Fundamentals and Advancements*; CRC Press: Boca Raton, FL, USA, 2019.
6. Thompson, M.K.; Moroni, G.; Vaneker, T.; Fadel, G.; Campbell, R.I.; Gibson, I.; Bernard, A.; Schulz, J.; Graf, P.; Ahuja, B. Design for Additive Manufacturing: Trends, opportunities, considerations, and constraints. *CIRP Ann.* **2016**, *65*, 737–760. [[CrossRef](#)]
7. Leach, R.; Carmignato, S. *Precision Metal Additive Manufacturing*; CRC Press: Boca Raton, FL, USA, 2020.
8. Bajaj, P.; Hariharan, A.; Kini, A.; Kürnsteiner, P.; Raabe, D.; Jäggle, E.A. Steels in additive manufacturing: A review of their microstructure and properties. *Mater. Sci. Eng. A* **2020**, *772*, 138633. [[CrossRef](#)]
9. DebRoy, T.; Wei, H.L.; Zuback, J.S.; Mukherjee, T.; Elmer, J.W.; Milewski, J.O.; Beese, A.M.; Wilson-Heid, A.; De, A.; Zhang, W. Additive manufacturing of metallic components—Process, structure and properties. *Prog. Mater. Sci.* **2018**, *92*, 112–224. [[CrossRef](#)]
10. Frazier, W.E. Metal Additive Manufacturing: A Review. *J. Mater. Eng. Perform.* **2014**, *23*, 1917–1928. [[CrossRef](#)]
11. Vafadar, A.; Guzzomi, F.; Rassau, A.; Hayward, K. Advances in metal additive manufacturing: A review of common processes, industrial applications, and current challenges. *Appl. Sci.* **2021**, *11*, 1213. [[CrossRef](#)]
12. Mazur, M.; Leary, M.; McMillan, M.; Elambasseril, J.; Brandt, M. SLM additive manufacture of H13 tool steel with conformal cooling and structural lattices. *Rapid Prototyp. J.* **2016**, *22*, 504–518. [[CrossRef](#)]
13. Legesse, F.; Kapil, S.; Vithasth, H.; Karunakaran, K.P. Additive manufacturing of H13 tooling element with conformal cooling channel using MIG cladding. *Int. J. Rapid Manuf.* **2018**, *7*, 1. [[CrossRef](#)]
14. Kahlert, M.; Brenne, F.; Vollmer, M.; Niendorf, T. Influence of Microstructure and Defects on Mechanical Properties of AISI H13 Manufactured by Electron Beam Powder Bed Fusion. *J. Mater. Eng. Perform.* **2021**, *30*, 6895–6904. [[CrossRef](#)]

15. Meng, Y.; Sugiyama, S.; Yanagimoto, J. Microstructural evolution during RAP process and deformation behavior of semi-solid SKD61 tool steel. *J. Mater. Process. Technol.* **2012**, *212*, 1731–1741. [[CrossRef](#)]
16. Pinkerton, A.J.; Li, L. Direct additive laser manufacturing using gas- and water-atomised H13 tool steel powders. *Int. J. Adv. Manuf. Technol.* **2004**, *25*, 471–479. [[CrossRef](#)]
17. Ma, M.; Wang, Z.; Zeng, X. A comparison on metallurgical behaviors of 316L stainless steel by selective laser melting and laser cladding deposition. *Mater. Sci. Eng. A* **2017**, *685*, 265–273. [[CrossRef](#)]
18. Stanford, M.; Kibble, K.; Lindop, M.; Mynors, D.; Durnall, C. An investigation into fully melting a maraging steel using direct metal laser sintering (DMLS). *Steel Res. Int* **2008**, *2*, 847–852.
19. Khairallah, S.A.; Anderson, A.T.; Rubenchik, A.; King, W.E. Laser powder-bed fusion additive manufacturing: Physics of complex melt flow and formation mechanisms of pores, spatter, and denudation zones. *Acta Mater.* **2016**, *108*, 36–45. [[CrossRef](#)]
20. Åsberg, M.; Fredriksson, G.; Hatami, S.; Fredriksson, W.; Krakhmalev, P. Influence of post treatment on microstructure, porosity and mechanical properties of additive manufactured H13 tool steel. *Mater. Sci. Eng. A* **2019**, *742*, 584–589. [[CrossRef](#)]
21. Yuan, M.; Cao, Y.; Karamchedu, S.; Hosseini, S.; Yao, Y.; Berglund, J.; Liu, L.; Nyborg, L. Characteristics of a modified H13 hot-work tool steel fabricated by means of laser beam powder bed fusion. *Mater. Sci. Eng. A* **2022**, *831*, 142322. [[CrossRef](#)]
22. Wang, M.; Wu, Y.; Wei, Q.; Shi, Y. Thermal Fatigue Properties of H13 Hot-Work Tool Steels Processed by Selective Laser Melting. *Metals* **2020**, *10*, 116. [[CrossRef](#)]
23. Janovec, J.; Výrostková, A.; Holý, A. Effect of tempering on development of carbide particles in 2.7 Cr-0.6 Mo-0.3 V steel. *J. Mater. Sci.* **1992**, *27*, 6564–6572. [[CrossRef](#)]
24. Katancik, M.; Mirzababaei, S.; Ghayoor, M.; Pasebani, S. Selective laser melting and tempering of H13 tool steel for rapid tooling applications. *J. Alloy. Compd.* **2020**, *849*, 156319. [[CrossRef](#)]
25. Krell, J.; Röttger, A.; Geenen, K.; Theisen, W. General investigations on processing tool steel X40CrMoV5-1 with selective laser melting. *J. Mater. Process. Technol.* **2018**, *255*, 679–688. [[CrossRef](#)]
26. Kim, J.-M.; Jin, H.-H.; Kwon, J.; Kang, S.H.; Lee, B.-S. Effects of cellular segregation for high strength and ductility of additively manufactured 304L stainless steel. *Mater. Charact.* **2022**, *194*, 112364. [[CrossRef](#)]
27. Wang, D.; Song, C.; Yang, Y.; Bai, Y. Investigation of crystal growth mechanism during selective laser melting and mechanical property characterization of 316L stainless steel parts. *Mater. Des.* **2016**, *100*, 291–299. [[CrossRef](#)]
28. Lei, F.; Wen, T.; Yang, F.; Wang, J.; Fu, J.; Yang, H.; Wang, J.; Ruan, J.; Ji, S. Microstructures and Mechanical Properties of H13 Tool Steel Fabricated by Selective Laser Melting. *Materials* **2022**, *15*, 2686. [[CrossRef](#)]
29. Han, Y.; Li, C.; He, S.; Gao, C.; Chen, S.; Li, E. Effect of Homogenisation Temperature on the Microstructure and Microhardness of As-Cast H13 Steel. *Met. Mater. Int.* **2021**, *28*, 755–769. [[CrossRef](#)]
30. Liu, F.; Fors, D.H.R.; Golpayegani, A.; André, H.-O.; Wahnström, G. Effect of Boron on Carbide Coarsening at 873 K (600 °C) in 9 to 12 pct Chromium Steels. *Metall. Mater. Trans. A* **2012**, *43*, 4053–4062. [[CrossRef](#)]
31. Godec, M.; Skobir Balantic, D.A. Coarsening behaviour of M23C6 carbides in creep-resistant steel exposed to high temperatures. *Sci. Rep.* **2016**, *6*, 29734. [[CrossRef](#)]
32. Hu, X.; Li, L.; Wu, X.; Zhang, M. Coarsening behavior of M23C6 carbides after ageing or thermal fatigue in AISI H13 steel with niobium. *Int. J. Fatigue* **2006**, *28*, 175–182. [[CrossRef](#)]
33. Krolczyk, G.; Feldshtein, E.; Dyachkova, L.; Michalski, M.; Baranowski, T.; Chudy, R. On the Microstructure, Strength, Fracture, and Tribological Properties of Iron-Based MMCs with Addition of Mixed Carbide Nanoparticulates. *Materials* **2020**, *13*, 2892. [[CrossRef](#)]
34. Feldshtein, E.E.; Dyachkova, L.N.; Królczyk, G.M. On the evaluation of certain strength characteristics and fracture features of iron-based sintered MMCs with nanooxide additives. *Mater. Sci. Eng. A* **2019**, *756*, 455–463. [[CrossRef](#)]
35. Zhu, Z.G.; Nguyen, Q.B.; Ng, F.L.; An, X.H.; Liao, X.Z.; Liaw, P.K.; Nai, S.M.L.; Wei, J. Hierarchical microstructure and strengthening mechanisms of a CoCrFeNiMn high entropy alloy additively manufactured by selective laser melting. *Scr. Mater.* **2018**, *154*, 20–24. [[CrossRef](#)]
36. Garcias, J.F.; Martins, R.F.; Branco, R.; Marciniak, Z.; Macek, W.; Pereira, C.; Santos, C. Quasistatic and fatigue behavior of an AISI H13 steel obtained by additive manufacturing and conventional method. *Fatigue Fract. Eng. Mater. Struct.* **2021**, *44*, 3384–3398. [[CrossRef](#)]
37. Silberschmidt, V.V. *Mechanics of Materials in Modern Manufacturing Methods and Processing Techniques*; Elsevier: Amsterdam, The Netherlands, 2020.
38. Marashi, J.; Yakushina, E.; Xirouchakis, P.; Zante, R.; Foster, J. An evaluation of H13 tool steel deformation in hot forging conditions. *J. Mater. Process. Technol.* **2017**, *246*, 276–284. [[CrossRef](#)]